Topological "Melting" of Cellular Domain Lattices in Magnetic Garnet Films

K. L. Babcock and R. M. Westervelt
Division of Applied Sciences and Department of Physics, Harvard University, Cambridge, Massachusetts 02138
(Received 9 May 1989)

We report observations of order-disorder phase transitions in metastable cellular patterns of magnetic domains at room temperature. The advance of a front destroys an ordered hexagonal domain lattice and leaves a topologically disordered cellular phase. Front motion is driven by stress in the domain patterns induced by an external bias field. The topological nature of the transitions gives rise to the novel features of particle (cell) nonconservation and irreversibility.

PACS numbers: 64.60.−i, 05.70.Fh, 75.70.Kw

The study of domain structure in uniaxial magnetic garnet films was originally motivated by their potential as magnetic bubble memories.[1] Recently, attention has been given to the rich spatial and temporal behavior exhibited by the two-dimensional patterns of magnetic domains supported by these films. Examples include the homogeneous coarsening of topologically disordered cellular patterns[2] and hysteretic undulation instabilities of stripe patterns[3] evolved in external bias fields.

In this Letter we report experimental observations of transitions between distinct phases of cellular domain patterns in garnet films at room temperature. The digitized photograph in Fig. 1 shows a well-defined front advancing and "melting" an ordered hexagonal domain lattice. Left behind is a disordered cellular "froth" phase with a diversity of cell shapes, areas, and numbers of nearest neighbors. Because the domain self-energies and interaction energies are much greater than kT, thermal effects are insignificant. The front is instead driven by domain lattice stress induced by an external bias field H_B, which serves as a control parameter analogous to temperature or pressure in the melting of solids. The collapse of the pentagonal domain structures that line the front in Fig. 1 mediate the topological changes associated with the melting. The experimental accessibility of the transitions allows us to determine the topological pathway between the ordered and disordered phases, a feature that may prove useful for understanding models of melting.

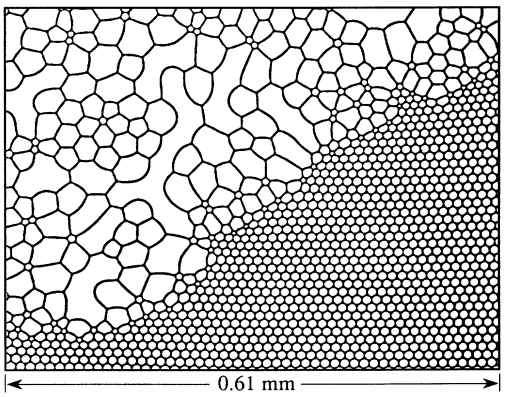

FIG. 1. Digitized photograph of "melting" front; $H_B = 79.7$ Oe. The collapse of the pentagonal bubble traps advances the front, destroying the hexagonal lattice phase and leaving behind the disordered froth phase of reduced cell density. The cell boundaries (dark areas) are comprised of magnetization aligned opposite to H_B.

We observed the transitions in a garnet film of composition $Fe_{3.91}Y_{1.20}Bi_{1.09}Gd_{0.95}Ga_{0.76}Tm_{0.09}O_{12}$, formulated at the Airtron Division of Litton Industries for use in magneto-optic devices.[4] A large literature[1] exists describing domain structure in such materials. Briefly, the Airtron garnet has bulk magnetization $4\pi M = 190$ G, film thickness $t = 7.8$ μm, Curie point $T_C = 170\,^{\circ}$C, and sufficient surface area to accommodate several million domains. The magnetic anisotropy is highly uniaxial with easy axis perpendicular to the film plane. The vertical domain walls between the "up" and "down" domains (those comprised of magnetization aligned with and opposite to H_B, respectively) are narrow (~ 0.1 μm) compared to the domain sizes (~ 10 μm), and have an effective surface energy $\sigma_W = 0.23$ erg/cm^2. The patterns are essentially two dimensional, and evolve by the lateral translation of the domain walls. The domains are observed via standard optical microscopy by utilizing the Faraday rotation of transmitted polarized light with an analyzer oriented to give contrast between the up and down domains. The domain images in the figures are high-resolution digitizations of high-contrast photographs, with white (black) areas correspondings to up (down) magnetization. For the transition data described here, cell densities were determined by computer analysis of digitized images, and an ac field component (frequency 40 Hz, amplitude 5 Oe) was applied in addition to the dc bias to minimize the effects of coercive friction[1] on the domain-wall motion; this technique is discussed in Ref. 2.

We produce the initial hexagonal lattice phase as follows: (i) A disordered "sea" of magnetic bubbles is nucleated via saturation and removal of an in-plane, 2.2-

kOe magnetic field. (ii) The bubble sea is annealed[5] by applying a spatially uniform ac magnetic field (40 Hz, 0–30 Oe) and a ~75-Oe dc component aligned opposite to the bubble magnetization. The ac field agitates the bubbles, and they order into polycrystalline lattices of variable, reproducible bubble densities. The average grain size increases with decreasing density, and ranges up to ~1 mm in diameter with a capacity of more than 10^4 bubbles. (iii) The ac field component is removed and the polarity of the dc bias H_B is slowly reversed to align with the bubble magnetization. The bubbles expand and squeeze the reversed magnetization, producing a cellular lattice that preserves the topology of the bubble lattice if H_B is not too large. We are able to obtain lattice cell densities in the range of 3000–6800 cells/mm^2. The maximum is set by the density of the original bubble sea, and the minimum by the run-out instability[1] of the bubbles which causes them to elongate and destroy the lattice during the reversal of the bias polarity.

The spatially uniform bias field H_B induces the melting of the polycrystalline hexagonal lattices. As described in detail in Ref. 2, H_B produces an effective tension in the cell walls that favors the reduction of the total cell-wall length. The hexagonal structure and the mutual repulsion of the reversed domains makes the ordered lattices stable. It is the unavoidable presence of topological defects, consisting of pairs of five- and seven-sided cells, triplets of eight-, five-, and five-sided cells, and chains of five- and seven-sided cells along the grain boundaries, that "poisons" the hexagonal lattice and initiates melting. Cell-wall tension causes the five-sided cells to shrink and form the small pentagonal structures seen in Fig. 1, referred to as bubble traps[2] because magnetic bubbles comprise their interiors. The bubble traps remain stable and resist complete collapse under a significant increase in bias field, and the domain configurations are pushed far from equilibrium with no topological change. However, a sufficient increase in H_B will eliminate a pentagonal bubble trap by producing local fields that destabililize the trapped bubble.[1,2] The associated topological changes result in neighboring cells with fewer than six sides that subsequently collapse, and the melting spreads and forms extended fronts such as that in Fig. 1.

We observe the fronts to advance by the topological mechanism illustrated in Fig. 2. In (a), the initial, high- and low-density phases are divided by a row of pentagonal bubble traps (shaded). In (b), the bubble traps have collapsed with uniform orientation, so that the six-sided cells along the front each gain one side. A topology-preserving rearrangement favored by cell-wall tension gives (c), identical to (a) but with the front advanced downward one cell width (arrow). In this model, the secondary phase is a compressed hexagonal lattice of density that is half of that in the initial phase. We observe the ordered structure of the model in Fig. 2 only

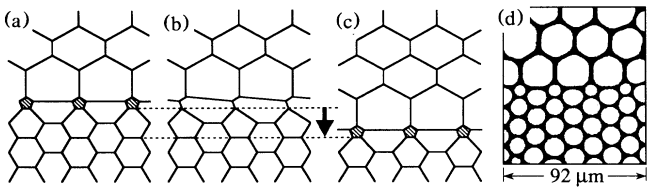

FIG. 2. (a)–(c) Model illustrating the topological mechanism of front propagation. (d) Section of an observed front with the same structure.

along short sections of fronts during transitions from lattices near the highest obtainable cell densities; an example is shown in the photograph in (d). The disorder always observed in the froth phase is generated when the collapse orientation of the pentagonal bubble traps along the front is nonuniform. For example, if the central bubble trap in Fig. 2 collapsed "to the left," instead of "to the right," the result would be a 5-7 cell pair in the froth phase rather than a pair of hexagons. Various combinations of collapse orientation produce a wide range of side numbers in the froth phase. Note that the pentagonal bubble traps help to preserve the Euler requirement[6] that the average number of sides of the cells must equal six along the front and in the froth. Cells with fewer than six sides generated at the front can subsequently collapse, typically within a few cell layers from the front. These secondary eliminations account for our observation that the cell density in the froth phase obeys $n_F < n_L/2$, where n_L is the density of the hexagonal lattice. We have never observed an increase in cell density as H_B is reduced. Because mutual domain repulsion prevents the inverses of the topological changes that accompany cell collapse,[2] the front motion, and the transition themselves, are irreversible.

We observe two melting regimes depending on the cell density in the ordered phase. For high-density lattices ($n_L > 4600$ cells/mm^2), the ordered and disordered phases coexist over a bias range Δ during the transition; an example is shown in Fig. 3. The photographs show stationary, metastable states formed by the coexisting phases as H_B is increased quasistatically. Stability is provided by the robust pentagonal bubble traps which, for fixed H_B, obstruct the advance of the fronts. The square data markers in the plot indicate the corresponding continuous drop in average cell density. Note the onset of melting at the defects and grain boundaries in photograph (a), and the gradual decrease in the area of the ordered regions [photographs (b)–(d)] similar to the heterogeneous melting of polycrystalline solids.[7] The cell density continues to decrease after the ordered regions are destroyed by the homogeneous coarsening of the froth phase.[2]

If $n_L < 4600$ cells/mm^2, the transitions are instead discontinuous, as shown by the circular data markers in Fig. 3. The sudden drop in cell density at $H_B = 79.7$ Oe corresponds to the front in Fig. 1. The fronts propagate

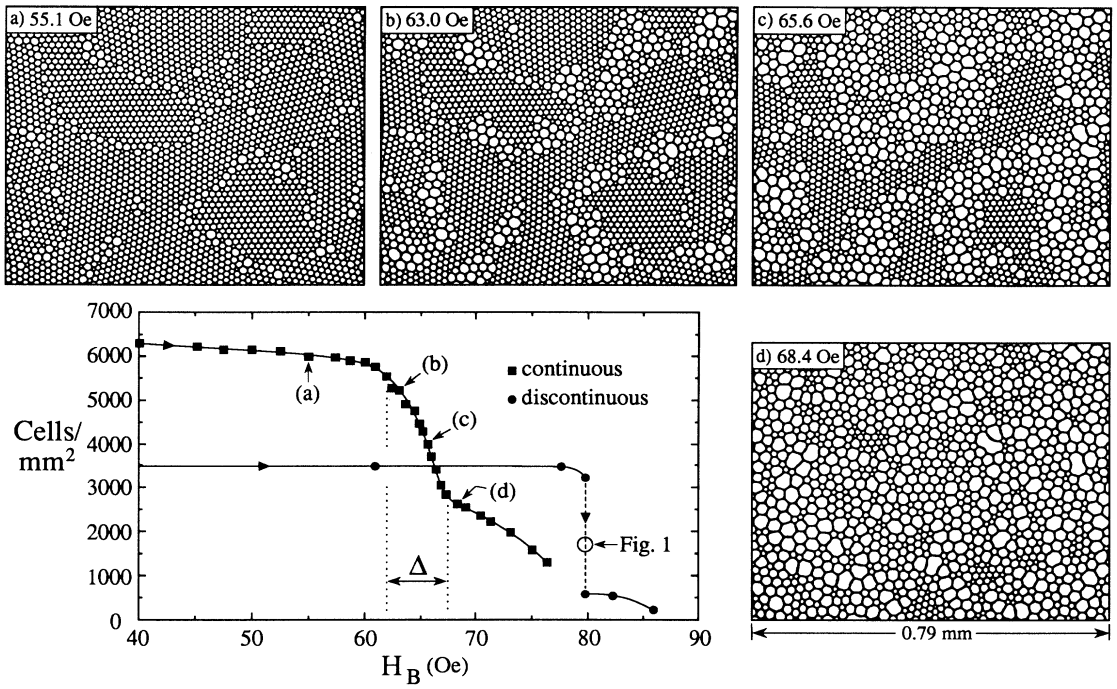

FIG. 3. Plot of evolution of average cell density under increasing bias field H_B. Square data markers correspond to stationary, metastable domain configurations in a continuous transition from an initial hexagonal lattice of density 6200 cells/mm^2. Ordered and disordered phases coexist over the bias range Δ. The photographs show domain configurations at selected field values of this transition. Circular data markers indicate the cell density involved from an initial lattice of density 3500 cells/mm^2. The discontinuous transition at $H_B = 79.7$ Oe corresponds to Fig. 1.

once formed, and a stationary, metastable state is not reached until the hexagonal lattice is completely destroyed. (To facilitate photography, the front in Fig. 1 was temporarily stopped by removing the ac field component.) The fraction of cells with six sides, an appropriate order parameter, also shows continuous and discontinuous drops with crossover at $n_L = 4600$ cells/mm^2.

Phase coexistence in the continuous transitions originates in the long-range (approximately dipole-dipole) interactions between the down domains mediated by their "stray" demagnetization fields. The condition for front advance can be expressed as[2] $H_B + H_S = H_P$, where H_S is the total stray field, and H_P is the local field sum required to destabilize the pentagonal bubble traps along the front. The stray fields H_S experienced by these bubble traps increase with cell density, and decrease as the lattice "islands" are eroded. The result is the observed sequence of metastable states with a continuous reduction in order as H_B increases. Discontinuous transitions arise when the relatively small stray fields originating in low-density lattices allow the bubble traps to survive to large enough H_B that the front remains unstable once melting is initiated.

Figure 4 shows an experimental "phase diagram" determined by evolving polycrystalline domain lattices covering the obtainable range of densities and corresponding grain sizes under increasing H_B. For each transition, we measured the following: (i) The minimum bias field required to completely destroy the ordered re-

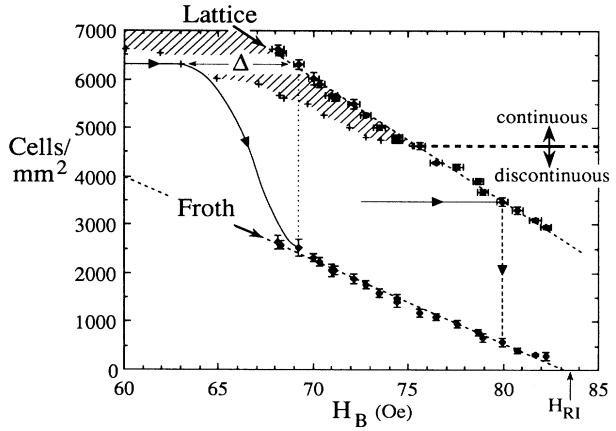

FIG. 4. Experimental "phase diagram." The vertical coordinate of a data point along the uppermost line is the cell density in the initial lattice phase; the horizontal coordinate is the corresponding "melting" field H_M. The lowest data line is the cell density of the froth phase. The width Δ of the hatched region indicates the bias range of two-phase coexistence in continuous transitions. Lines with arrows show schematically the evolution of average cell density in continuous and discontinuous transitions.

gions, which we refer to as the "melting" field H_M. These values make up the phase boundary shown as the uppermost line of data. The vertical coordinate of a data point is the cell density in the initial hexagonal lattice, and the horizontal coordinate is H_M. (ii) The onset of melting in the continuous transitions, marked by crosses paired horizontally along lines of constant cell density with points on the phase boundary. The width Δ of the shaded region indicates the bias range of phase coexistence. The crossover from continuous to discontinuous melting at $n_L \approx 4600$ cells/mm^2 corresponds to $H_M \approx 76$ Oe. (iii) The cell density of the resulting froth phases, shown as the lowest line of data; these points are paired vertically with those on the phase boundary.

Figure 4 shows a discrete drop in cell density for both continuous and discontinuous transitions. Relative to the saturated (single domain) state, the total domain configuration energy is[1] $E_T = E_W + E_D + E_I$, where E_W is the domain-wall energy, E_D is the demagnetization field energy, and E_I is the energy of interaction of the magnetization with H_B. For fixed bias, E_T is a continuous function of domain spacing[2,8] or equivalently, cell density. The energies E_T of the two phases are thus unequal, including those in the coexistence region of continuous transitions. Both the continuous and discontinuous transitions are "first order" in the sense that the drop in cell density reduces E_T. We emphasize that it is the robust pentagonal bubble traps that initially obstruct the topological evolution and allow the lattices to survive to nonequilibrium bias regimes before the onset of melting.

Figure 4 also shows that the froth density n_F and the melting field H_M vary continuously and approximately linearly with the lattice cell density n_L. The linearity appears to originate in the additive condition $H_B + H_S = H_P$ for front advance and the dependence $H_L \propto n_L$, where H_L is the contribution of the lattice to the stray field H_S. However, this simple scaling ignores the contribution of the froth phase to H_S and the dependence of H_L and H_P on cell-wall width; the linearity of the phase boundary is therefore somewhat surprising. Less so is the location of the intercept $n_F = 0$ at $H_M = 83.2$ Oe, close to the run-in field $H_{RI} = 83.5$ Oe[1,2] of stripe domains in the Airtron garnet. The energy per unit length of an isolated, infinitely long stripe domain approaches zero as $H_B \rightarrow H_{RI}$, and the average cell area in minimum-energy cellular patterns diverges.[2] Transitions from lattices with the minimum obtainable n_L thus result in froths near equilibrium.

We would like to thank Raymond Wolfe and James Sethna for helpful discussions, and Roger Belt and the Airtron Division of Litton Industries for supplying the garnet sample. This work was supported by the Office of Naval Research under Contracts No. N00014-84-K-0329 and No. N00014-84-K-0465.

[1]See, for example, A. P. Malozemoff and J. C. Slonczewski, *Magnetic Domain Walls in Bubble Materials* (Academic, New York, 1979); A. H. Eschenfelder, *Magnetic Bubble Technology* (Springer-Verlag, New York, 1981), and references therein.

[2]K. L. Babcock and R. M. Westervelt, "Elements of Cellular Domain Patterns in Magnetic Garnet Films" [Phys. Rev. A (to be published)].

[3]P. Molho, J. Gouzerh, J. C. S. Levy, and J. L. Porteseil, J. Magn. Magn. Mater. **54-57**, 857 (1987).

[4]R. F. Belt and J. B. Ings, Proc. SPIE Int. Soc. Opt. Eng. **753**, 142 (1987).

[5]G. R. Woolhouse and P. Chaudhari, Philos. Mag. **31**, 161 (1974).

[6]For a review of cellular systems, see D. Weaire and N. Rivier, Contemp. Phys. **25**, 59 (1984).

[7]See, for example, N. G. Ainslie, J. D. Mackenzie, and D. Turnbull, J. Phys. Chem. **65**, 1718 (1961).

[8]J. A. Cape and G. W. Lehman, J. Appl. Phys. **42**, 5732 (1971).